Eur. Phys. J. B **41**, 345–363 (2004)
DOI: 10.1140/epjb/e2004-00328-1

THE EUROPEAN PHYSICAL JOURNAL B

A parsimonious and universal description of turbulent velocity increments

O.E. Barndorff-Nielsen[a], P. Blæsild, and J. Schmiegel

Department of Mathematical Sciences, University of Aarhus, 8000 Aarhus, Denmark

Received 24 February 2004 / Received in final form 13 August 2004
Published online 21 October 2004 –

Abstract. This paper proposes a reformulation and extension of the concept of Extended Self-Similarity. In support of this new hypothesis, we discuss an analysis of the probability density function (pdf) of turbulent velocity increments based on the class of normal inverse Gaussian distributions. It allows for a parsimonious description of velocity increments that covers the whole range of amplitudes and all accessible scales from the finest resolution up to the integral scale. The analysis is performed for three different data sets obtained from a wind tunnel experiment, a free-jet experiment and an atmospheric boundary layer experiment with Taylor-Reynolds numbers $R_\lambda = 80, 190, 17000$, respectively. The application of a time change in terms of the scale parameter δ of the normal inverse Gaussian distribution reveals some universal features that are inherent to the pdf of all three data sets.

PACS. 47.27.-i Turbulent flows, convection, and heat transfer

1 Introduction

Since the pioneering work of Kolmogorov [1–3] and Obukhov [4–6], intermittency of the turbulent velocity field plays a central role in turbulence research. Intermittency refers to the fact that fluctuations around the mean velocity occur in clusters and are more violent than expected from Gaussian statistics. Furthermore, the frequency of large fluctuations increases with increasing resolution. In terms of moments of velocity increments $u(s) \equiv v(\sigma + s) - v(\sigma)$, intermittency in turbulence is usually described by approximate multifractal scaling of structure functions

$$\mathrm{S}_n(s) = \mathrm{E}\{(v(\sigma + s) - v(\sigma))^n\} \propto |s|^{\tau(n)}. \qquad (1)$$

Here, $v(\sigma)$ is one component of the velocity (usually along the mean flow) at position σ and the lag s is within the so-called inertial range. The inertial range is defined as the range of scales where the spectrum $E(k)$ (the Fourier transform of the correlation function of the velocity field) displays a power law $E(k) \propto k^{-5/3}$ [4,5,7]. The term multifractal scaling is due to the non-linear dependence of the scaling exponents $\tau(n) > 0$ on the order n.

Multifractal scaling of velocity increments is assumed to hold in the limit of infinite Reynolds number. However, experiments show that the scaling behaviour (1) might be poor, even for large Reynolds numbers [8,9]. Furthermore, even if the scaling relation (1) holds, the inertial range still covers only part of the accessible scales where intermittency is observed.

One way to improve the characterization of intermittency by means of (1) consists of applying the concept of Extended Self-Similarity (ESS) introduced by Benzi et al. [10]. Plotting structure function of order n against those of some order $n' < n$ improves the accuracy of (1) in most cases and leads to an extension of the scaling range. The theoretical foundation of this effect is not understood in detail.

In Section 5 we propose a reformulation and extension of ESS in the form of a stochastic equivalence relation. In support of this hypothesized relation we provide, in Sections 3 and 4, the results of a detailed analysis of three main data sets.

From a probabilistic point of view, (1) expresses a scaling relation for the moments of the probability density function (pdf) of velocity increments. A proper estimation of higher-order moments requires an accurate estimation of the tails of the pdf. Thus it may be advantageous to directly work with the pdf. In terms of the pdf, intermittency refers to the increase of the non-Gaussian behaviour of the pdf of velocity increments with decreasing lag.

A typical scenario is characterized by a Gaussian shape for the large scales (larger than scales at the inertial range), turning to exponential tails within the inertial range and stretched exponential tails for dissipation scales (below the inertial range). This change of shape across all scales clearly reveals the inadequacy of a characterization of intermittency solely via multifractal scaling of

[a] e-mail: oebn@imf.au.dk

structure functions (which is observed only within the inertial range).

A detailed parsimonious description of the pdf of velocity increments not only contributes to a basic understanding of intermittency in turbulence, but also has important applications in engineering problems. Its relevance for the description of turbulent combustion and other applications was discussed in detail by Kuznetsov and Sabelnikov [11].

Existing work about the pdf of velocity increments concentrates on a description of the tails of the pdf or characterizes the pdf only within the inertial range.

Exponential tails $\propto \exp(-b(s)u)$ for the pdf of velocity increments with lags s within the inertial range are reported in [12–14]. A detailed investigation of the logarithmic decrement $b(s)$ as a function of the lag s is performed in [15]. They propose a power-law $b(s) \propto s^{\beta}$ with $\beta \approx 0.17$ as a reasonable fit within the inertial range. [16–19] extend the description of the tails from exponentials to stretched exponentials $\propto \exp(bu^m)$ to include dissipative scales below the inertial range and integral scales above the inertial range. The stretching exponent m appears to vary continuously from 0.5 in the dissipation range up to 2 for integral scales [17]. [20] reports stretched exponential tails with stretching exponents m restricted to $m \geq 1$ for a flow between concentric cylinders at Reynolds numbers where there is no inertial range, i.e. no scaling of the spectrum. [21,22] compare the tails of the pdf of longitudinal (where the lag s is along the direction of the mean flow) and transversal velocity increments (where the lag s is perpendicular to the direction of the mean flow) and find stretched exponentials in both cases.

There are a number of theoretical models that incorporate the exponential behaviour of the tails of the pdf of velocity increments and attempt to describe the inertial range statistics for all amplitudes of the velocity field. Most of these are based on the multifractal description and thus restricted to the inertial range.

[23] connects the multifractal scaling of absolute velocity increments $|u(s)|$ with Gaussian large scale fluctuations and derive a superposition of stretched exponentials for the pdf of velocity increments with lags s within the inertial range. In this and similar approaches, the observed skewness of velocity increments (which is due to a stretching of vortex lines and relates to the energy transfer towards small scales) is neglected. A similar approach with a discrete superposition of Gaussian distributions is proposed in [17].

In [24], moments of absolute velocity increments are linked to the pdf by a simple integral relation. Using an asymptotic relation, the non-skewed, i.e. symmetrized, pdf can be constructed from the multifractal scaling spectrum $\tau(n)$.

Castaing et al. [12] start from the log-normal model of Kolmogorov [3] and Obukhov [6]. They fit the variance of the scale-dependent energy dissipation rate ϵ by a power law and assume all quantities conditioned on fixed ϵ as being Gaussian. In this framework they find a superposition of Gaussian distributions with log-normal variances as an empirical model for the non-skewed inertial-range pdf.

[25–30] combine the multifractality of velocity increments with statistics that are constructed from generalized measures of entropy, i.e. extensive Rényi or non-extensive Tsallis entropy. The multifractal aspect of their analysis again restricts to inertial range statistics.

[31] use an approach that is not based on multifractality of velocity increments. They derive numerically the pdf of velocity increments from a Fokker-Planck approach that includes the observed skewness of the pdf. However, the Markov-hypothesis of the velocity field breaks down for scales below the Taylor scale which is within the inertial range. Thus they are not able to include dissipation scale statistics.

In summary, these references focus on the tails, on the inertial range and/or on absolute velocity increments.

According to [7], it is an open question whether different ranges of scales (dissipative, inertial and integral scales) require different functional forms of the pdf of velocity increments or whether it is possible to find one functional form for the pdf that is varying continuously with the scale.

The present work answers this question in favour of a unified description at all scales. We provide an empirical description of the skewed pdf of velocity increments that covers all accessible scales and provides a reasonable fit for all amplitudes within one tractable class of distributions. It turns out that normal-inverse Gaussian (NIG) distributions are flexible enough to achieve this goal with high accuracy.

Section 2.1 gives a summary of the mathematical properties of NIG distributions, and Section 2.2 provides a summary of the type of data we analyse. Section 3 and Section 4 contain the main results. The pdf of velocity increments for all lags and all amplitudes can be fitted within the four-parameter class of NIG distributions. The quality of the fit is independent of the lag s and independent of the kind of experiment. We also perform an analysis of the tails of the pdf in terms of stretched exponentials; the estimates of the stretching exponents m as a function of the lag s are in conformity with classical findings. The variability features of the four parameters are examined in more detail in Section 4. The use of the scale parameter δ of the NIG distribution as a generic time change reveals some universal features for the remaining parameters of the NIG distributions and for the stretching exponents m that describe the tails. Section 5 discusses some implications of our empirical findings and establishes the connection to ESS. In particular, we show that ESS can be viewed as an immediate consequence of a stochastic equivalence relation that connects the statistics of velocity increments of different experiments and different Reynolds numbers. Section 6 concludes.

2 Background

This section gives a brief overview of the mathematical properties of the normal inverse Gaussian distribution,

that are essential for the analysis performed in subsequent sections. We also provide a brief description of the kind of data we use for our analysis.

2.1 NIG distributions

The normal inverse Gaussian law, with parameters α, β, μ and δ, is the distribution on the real axis $\mathbf{R}$ having probability density function

$$p(x;\alpha,\beta,\mu,\delta) = a(\alpha,\beta,\mu,\delta)q\left(\frac{x-\mu}{\delta}\right)^{-1} \times K_1\left\{\delta\alpha q\left(\frac{x-\mu}{\delta}\right)\right\}e^{\beta x} \quad (2)$$

where $q(x) = \sqrt{1+x^2}$ and

$$a(\alpha,\beta,\mu,\delta) = \pi^{-1}\alpha\exp\left\{\delta\sqrt{\alpha^2-\beta^2}-\beta\mu\right\} \quad (3)$$

and where K_1 is the modified Bessel function of the third kind and index 1. The domain of variation of the parameters is given by $\mu \in \mathbf{R}$, $\delta \in \mathbf{R}_+$, and $0 \le |\beta| < \alpha$. The distribution is denoted by $\mathrm{NIG}(\alpha,\beta,\mu,\delta)$.

If X is a random variable with distribution $\mathrm{NIG}(\alpha,\beta,\mu,\delta)$ then the cumulant generating function of X, i.e. $K(\theta;\alpha,\beta,\mu,\delta) = \log E\{e^{\theta X}\}$, has the form

$$K(\theta;\alpha,\beta,\mu,\delta) = \delta\left\{\sqrt{\alpha^2-\beta^2}-\sqrt{\alpha^2-(\beta+\theta)^2}\right\}+\mu\theta. \quad (4)$$

It follows immediately from this that if $x_1, ..., x_m$ are independent normal inverse Gaussian random variables with common parameters α and β but individual location-scale parameters μ_i and δ_i $(i = 1, ..., m)$ then $x_+ = x_1 + ... + x_m$ is again distributed according to a normal inverse Gaussian law, with parameters $(\alpha, \beta, \mu_+, \delta_+)$.

Furthermore, the first four cumulants of $\mathrm{NIG}(\alpha,\beta,\mu,\delta)$, obtained by differentiation of (4), are found to be

$$\kappa_1 = \mu + \frac{\delta\rho}{\sqrt{1-\rho^2}}, \quad \kappa_2 = \frac{\delta}{\alpha(1-\rho^2)^{3/2}} \quad (5)$$

and

$$\kappa_3 = \frac{3\delta\rho}{\alpha^2(1-\rho^2)^{5/2}}, \quad \kappa_4 = \frac{3\delta(1+4\rho^2)}{\alpha^3(1-\rho^2)^{7/2}}, \quad (6)$$

where $\rho = \beta/\alpha$. Hence, the standardised third and fourth cumulants are

$$\bar\kappa_3 = \frac{\kappa_3}{\kappa_2^{3/2}} = 3\frac{\rho}{\{\delta\alpha(1-\rho^2)^{1/2}\}^{1/2}}$$
$$\bar\kappa_4 = \frac{\kappa_4}{\kappa_2^2} = 3\frac{1+4\rho^2}{\delta\alpha(1-\rho^2)^{1/2}}. \quad (7)$$

We note that the NIG distribution (2) has semiheavy tails; specifically,

$$p(x;\alpha,\beta,\mu,\delta) \sim \text{const.}\,|x|^{-3/2}\exp\left(-\alpha|x|+\beta x\right), \quad x \to \pm\infty \quad (8)$$

as follows from the asymptotic relation

$$K_\nu(x) \sim \sqrt{2/\pi}x^{-1/2}e^{-x} \quad \text{as} \quad x \to \infty. \quad (9)$$

The normal inverse Gaussian law $\mathrm{NIG}(\alpha,\beta,\mu,\delta)$ has the following important characterisation in terms of the bivariate Brownian motion with drift. Let $B(t) = \{B_1(t), B_2(t)\}$ be a bivariate Brownian motion starting at $(\mu, 0)$ and having drift vector (β, γ) where $\beta \in \mathbf{R}$ and $\gamma \ge 0$. Furthermore, let T denote the time when B_1 first reaches level $\delta > 0$ and let $X = B_2(T)$. Then $X \sim \mathrm{NIG}(\alpha,\beta,\mu,\delta)$ with $\alpha = \sqrt{\beta^2+\gamma^2}$.

It is often of interest to consider alternative parametrisations of the normal inverse Gaussian laws. In particular, letting $\bar\alpha = \delta\alpha$ and $\bar\beta = \delta\beta$, we have that $\bar\alpha$ and $\bar\beta$ are invariant under location—scale changes.

NIG shape triangle For some purposes it is useful, instead of the classical skewness and kurtosis quantities (7), to work with the alternative asymmetry and steepness parameters χ and ξ defined by

$$\chi = \rho\xi \quad (10)$$

and

$$\xi = (1+\bar\gamma)^{-1/2} \quad (11)$$

where $\rho = \beta/\alpha = \bar\beta/\bar\alpha$ and $\bar\gamma = \delta\gamma = \delta\sqrt{\alpha^2-\beta^2}$. Like $\bar\kappa_3$ and $\bar\kappa_4$, these parameters are invariant under location-scale changes and the domain of variation for (χ, ξ) is the *normal inverse Gaussian shape triangle*

$$\{(\chi,\xi) : -1 < \chi < 1, 0 < \xi < 1\}.$$

The distributions with $\chi = 0$ are symmetric, and the normal and Cauchy laws occur as limiting cases for (χ, ξ) near to $(0, 0)$ and $(0, 1)$, respectively. Figure 1 gives an impression of the shape of the NIG distributions for various values of (χ, ξ).

Note in this connection that $\bar\kappa_3$ and $\bar\kappa_4$ may be reexpressed as

$$\bar\kappa_3 = 3\bar\gamma^{-1}\frac{\rho}{\{(1+\rho^2)(1-\rho^2)^{1/2}\}^{1/2}}$$

and

$$\bar\kappa_4 = 3\bar\gamma^{-1}\frac{1+4\rho^2}{(1-\rho^4)^{1/2}}$$

from which it follows that for small ρ we have approximately $\xi \doteq (1+3/\bar\kappa_4)^{-1/2}$ and $\bar\kappa_3 \doteq \rho\bar\kappa_4$ (compare to (10)); Thus the roles of χ and ξ are rather similar to those of the classical quantities $\bar\kappa_3$ and $\bar\kappa_4$. Note also that ρ may be considered as an alternative asymmetry parameter, see Figure 1; this is of some particular interest in turbulence, cf. Section 4.1.

A systematic study of the class of normal inverse Gaussian distributions, and of associated stochastic processes, was begun in [32–36]. Further theoretical developments and applications are discussed in [37–48]. As discussed in the papers cited and in references given there,

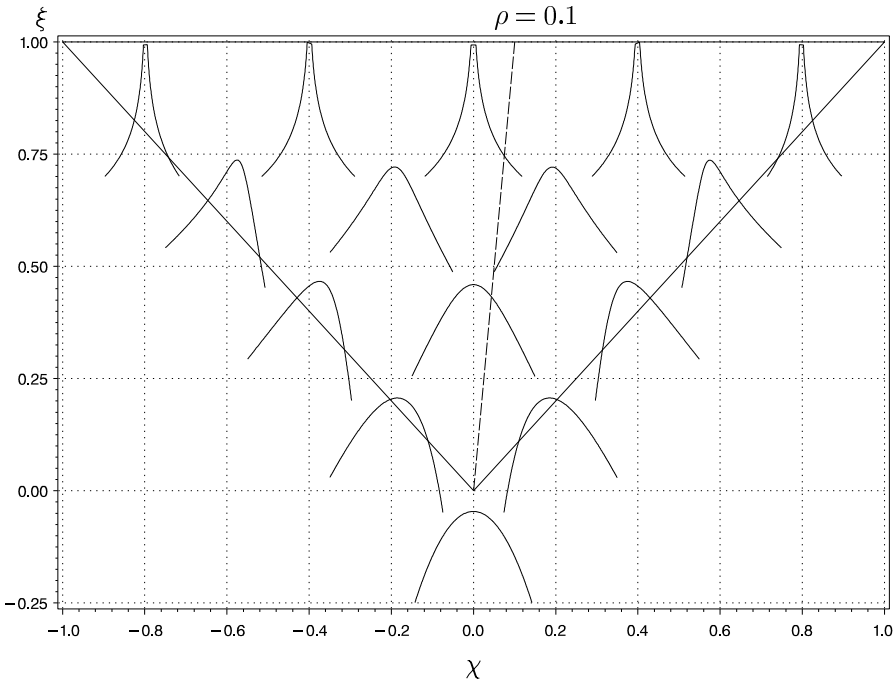

Fig. 1. The shape triangle of the *normal inverse Gaussian distributions (NIG distributions)* with the log density functions of the standardized distributions, i.e. with mean 0 and variance 1, corresponding to the values $(\chi, \xi) = (\pm 0.8, 0.999)$, $(\pm 0.4, 0.999)$, $(0.0, 0.999)$, $(\pm 0.6, 0.75)$, $(\pm 0.2, 0.75)$, $(\pm 0.4, 0.5)$, $(0.0, 0.5)$, $(\pm 0.2, 0.25)$ and $(0.0, 0.0)$. The coordinate system of the log densities is placed at the corresponding value of (χ, ξ) with the scale being 1/20 of the original. Furthermore, the line corresponding to $\rho = 0.1$, i.e. $\chi = 0.1\xi$, is shown.

the class of NIG distributions and processes have been found to provide accurate modelling of a great variety of empirical findings in the physical sciences and in financial econometrics. (The wider class of generalised hyperbolic distributions, introduced in [49], provides additional possibilities for realistic modelling of dynamical processes, see references in the papers cited above.)

2.2 Description of the data

Our analysis of the relevance of NIG distributions for turbulent velocity increments is based on three data sets obtained from three different experiments. In the following, we will refer to these data sets using the abbreviations data set I for the atmospheric boundary layer experiment, data set II for the free-jet experiment and data set III for the wake-flow experiment. We only give a brief description of the experiments and list in Table 1 as the main parameters the Reynolds number R_λ based on the Taylor microscale, the mean velocity U, the sampling frequency f and the estimated decorrelation time T. For more details, we refer to [50,51] for data set I, [31] for data set II and [52] for data set III.

Data set I consists of the one point time record of the longitudinal (along the mean flow) velocity-component in the atmospheric boundary layer at a height of 35 m above the ground. The total size of the record is 2×10^7.

Data set II consists of the one point time record of the longitudinal velocity-component in a free-jet experiment.

Table 1. Characteristic parameters Reynolds number R_λ, U (unit m/s), f (unit kHz) and T (in units of the finest resolution $1/f$) for the three data sets.

Characteristic parameters				
data set	R_λ	U	f	T
I	17000	8.3	5	20000
II	190	2.26	8	240
III	80	5.13	10	50

A jet of dry air, continuously streaming into the experimental chamber through a nozzle, develops in a surrounding of dry air which is in rest. Shear forces which arise at the edge of the jet lead to growing instabilities and finally turbulence. The time series was measured in the middle of the jet at a distance, where fluctuations around the mean can be assumed to be homogeneous, isotropic and stationary. The total number of records is 12.5×10^6.

Data set III consists of the one point time record of the longitudinal velocity-component in a wake generated by a flat plate, normal to the flow and placed downstream in the contraction of an open circuit wind tunnel. The total sample size is 4.2×10^6.

For the estimation of the pdf of velocity increments we normalized each of the velocity records by its standard deviation. Furthermore, we divided each data set, for each lag, into non-overlapping subsets of equal length and calculated the velocity increments at the center of each subset, i.e. the analyzed data for each lag s are of the form $v((2i-1)L/2+s/2) - v((2i-1)L/2-s/2), i = 1, \ldots, N_L$.

Table 2. Description of the data used to estimate the pdf of velocity increments.

Sample characteristics			
data set	$s \in$	L	N_L
I	$[4, 280]$	400	50000
	$[300, 680]$	800	25000
	$[700, 1500]$	1600	12500
	$[1600, 3800]$	4000	5000
	$[4000, 9500]$	10000	2000
II	$[2, 200]$	250	50000
	$[220, 380$	500	25000
	$[400, 880]$	1000	12500
III	$[2, 102]$	130	30000

Table 2 lists the length L of the subsets and the sample size N_L for each lag s (in units of the finest resolution $1/f$).

3 Distribution of velocity increments

In this section, we examine the pdf of temporal velocity increments

$$u(s) \equiv v(t+s) - v(t) \tag{12}$$

for all three data sets, where t and the temporal lag s are measured in units of the finest temporal resolution $1/f$ and f is the sampling frequency. Note that we are not using Taylor's frozen flow hypothesis [7], which would translate (12) into $v(\sigma - Us) - v(\sigma)$, where U is the mean velocity and σ denotes the spatial position. With our definition (12) of velocity increments we expect a positively skewed pdf according to the reversed sign of the famous Kolmogorov 4/5 th law [1,2].

As the main result of this section we state that the pdf of temporal velocity increments can well be fitted by a normal inverse Gaussian distribution for all amplitudes and all temporal lags s, ranging from the finest resolution $1/f$ up to the largest lags, where a proper statistical inference is feasible.

3.1 NIG analysis

The analysis of the pdf of the turbulent velocity increments, from the data described in Section 2.2, is performed using maximum likelihood estimation of the four parameters α, β, μ and δ of the NIG$(\alpha, \beta, \mu, \delta)$ distribution. The numerical estimation uses the routine "hyp", a program consisting of various numerical and graphical procedures for assessing the reasonableness of an analysis using one of the generalised hyperbolic distributions, in particular the NIG distribution. It provides the estimates of the parameters of the NIG distribution and evaluates the agreement between the observed and the estimated distribution.

Figures 2–4 illustrate, by examples, the results of the approximation of the empirical pdf of velocity increments within the class of NIG distributions for our three data sets. The lags shown in Figures 2–4 vary over the whole range of lags that allow for a proper estimation of the empirical pdf. The largest lags are well inside the Gaussian regime for data sets II and III, while for data set I the Gaussian limit is not reached. For the lags allowing proper estimation but which are not represented in these Figures the accuracy of the approximation is equally good. Results for those lags can be downloaded from `http://home.imf.au.dk/schmiegl/NIG`.

The overall impression we get from Figures 2–4 strongly supports the relevance of NIG distributions for describing the pdf of velocity increments for all lags s. The quality of the fit is independent of the kind of data and independent of the lag s. Discrepancies between the NIG approximation and the empirical pdf occur for large amplitudes where the pdf become approximately $\lesssim 10^{-6}$. The deviations at large amplitudes show up when the scatter of the data becomes visible and thus we may expect the goodness of fit to increase with increasing sample size.

The analysis within the class of NIG distributions clearly exhibits the well-known characteristics of the evolution of the pdf of velocity increments across all lags. For data set I and II we observe stretched exponentials within the dissipative scales, turning to exponential tails and finally reaching Gaussian-like shapes for the very large lags. For data set III we do not observe convex stretched exponentials but a smooth change from exponential tails to Gaussian tails. This observation is in conformity with results reported in [20] where the absence of convex stretched exponentials for the tails is connected to the absence of an inertial range.

To complete the analysis of this section we show the parameters $\alpha(s)$, $\beta(s)$, $\mu(s)$ and $\delta(s)$ of the fitted NIG$(\alpha(s), \beta(s), \mu(s), \delta(s))$ distributions in Figure 5. Leaving aside the scatter at large lags, all parameters roughly follow a smooth curve with comparable range of values. The estimated parameters for data sets II and III seem to have a similar dependence on the lag s while data set I shows a different behaviour, in particular for the parameters $\alpha(s)$ and $\beta(s)$. This is not surprising since the Reynolds numbers of data sets II and III are comparable in order. In Section 4, we propose useful combinations of these parameters that clearly indicate universal features, common to all three data sets, that are hidden in Figure 5.

3.2 Stretched exponential tails

The analysis of the pdf of velocity increments based on the class of NIG distributions in the last Section showed the evolution from convex tails for small lags through exponential tails for moderate lags and finally to Gaussian-like tails for large lags (Figs. 2–4). For comparison with classical findings we now quantify these observations in terms of stretched exponential tails

$$p(u) \propto \exp\{bu^m\} \tag{13}$$

for large amplitudes u. We somewhat arbitrarily define large amplitudes u for a given lag s as increments that exceed 10% of the largest observed amplitude. We

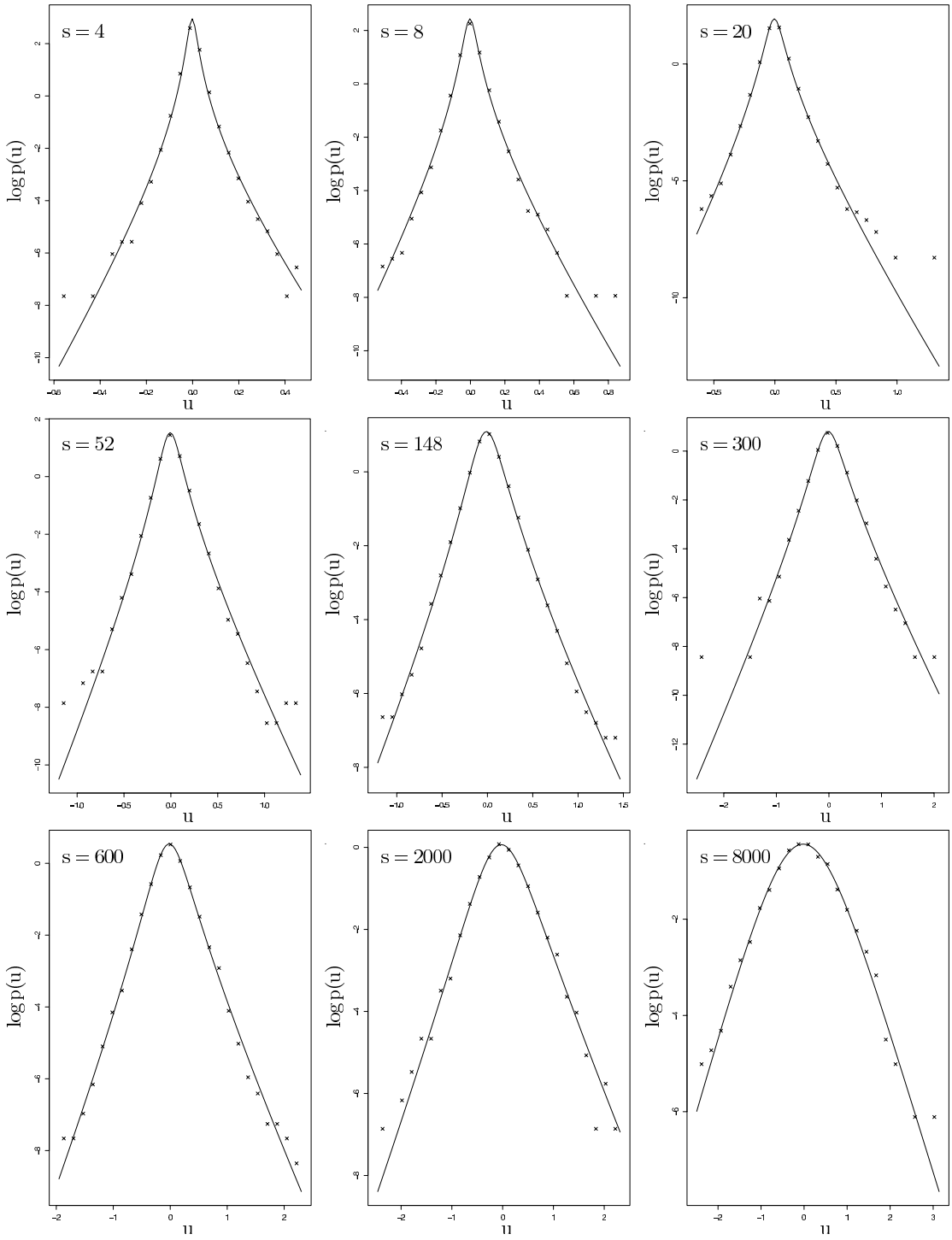

Fig. 2. Approximation of the pdf of velocity increments within the class of NIG distributions for data set I and lags $s = 4, 8, 20, 52, 148, 300, 600, 2000, 8000$ (in units of the finest resolution $1/f$).

performed a least mean square fit for the stretching exponent m in (13) for the right tail of the NIG distributions for lags that correspond to those in Figures 2–4. We observed stretched exponentials of the form (13) for all lags and the whole range of large amplitudes in conformity with results reported in the literature.

These findings are not in contrast to the stated asymptotically semiheavy tails (8) for NIG distributions. Semiheavy tails occur at very large amplitudes which do not appear in our analysis. The observed stretched exponentials (13) describe intermediate amplitudes. In this respect it is to note that [21] give some arguments in favour of only

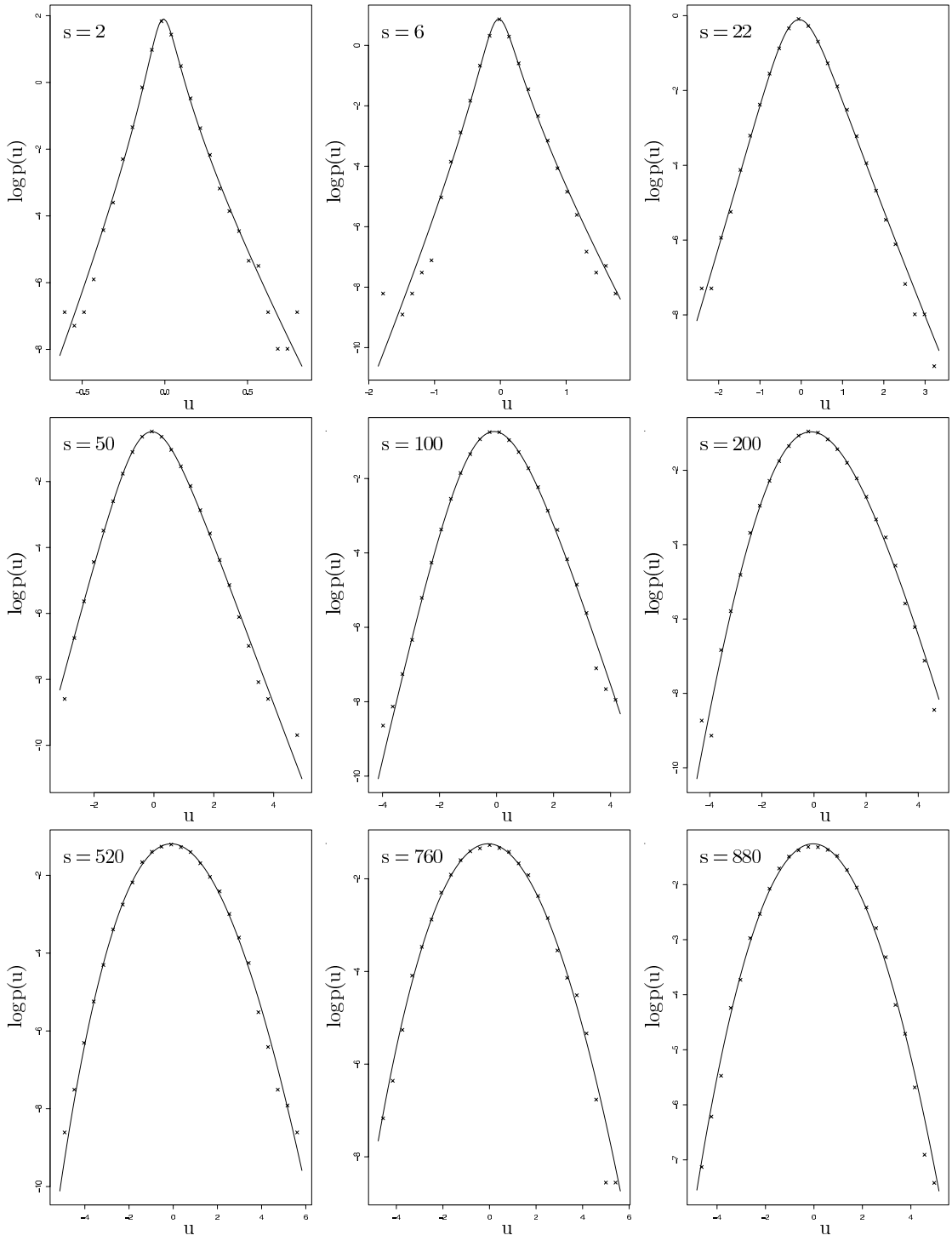

Fig. 3. Approximation of the pdf of velocity increments within the class of NIG distributions for data set II and lags $s = 2, 6, 22, 50, 100, 200, 520, 760, 880$ (in units of the finest resolution $1/f$).

a finite range of amplitudes with stretched exponential behaviour for turbulent velocity data.

Figure 6a shows the estimated stretching exponents m as a function of the lag s. For data set I, the largest observed stretching exponent is clearly below the Gaussian value 2, which indicates that the large scale limit of data set I is away from Gaussianity. We come back to this kind of behaviour in Section 4.1 where we investigate the global shape of the pdf in more detail. For data sets II and III the stretching exponent reaches the Gaussian limit but does not display the strong convexity of the pdf of data set I.

The overall impression of Figure 6a does not reveal any universal behaviour between the three data sets. However, Figure 6b shows the same stretching exponents m but now

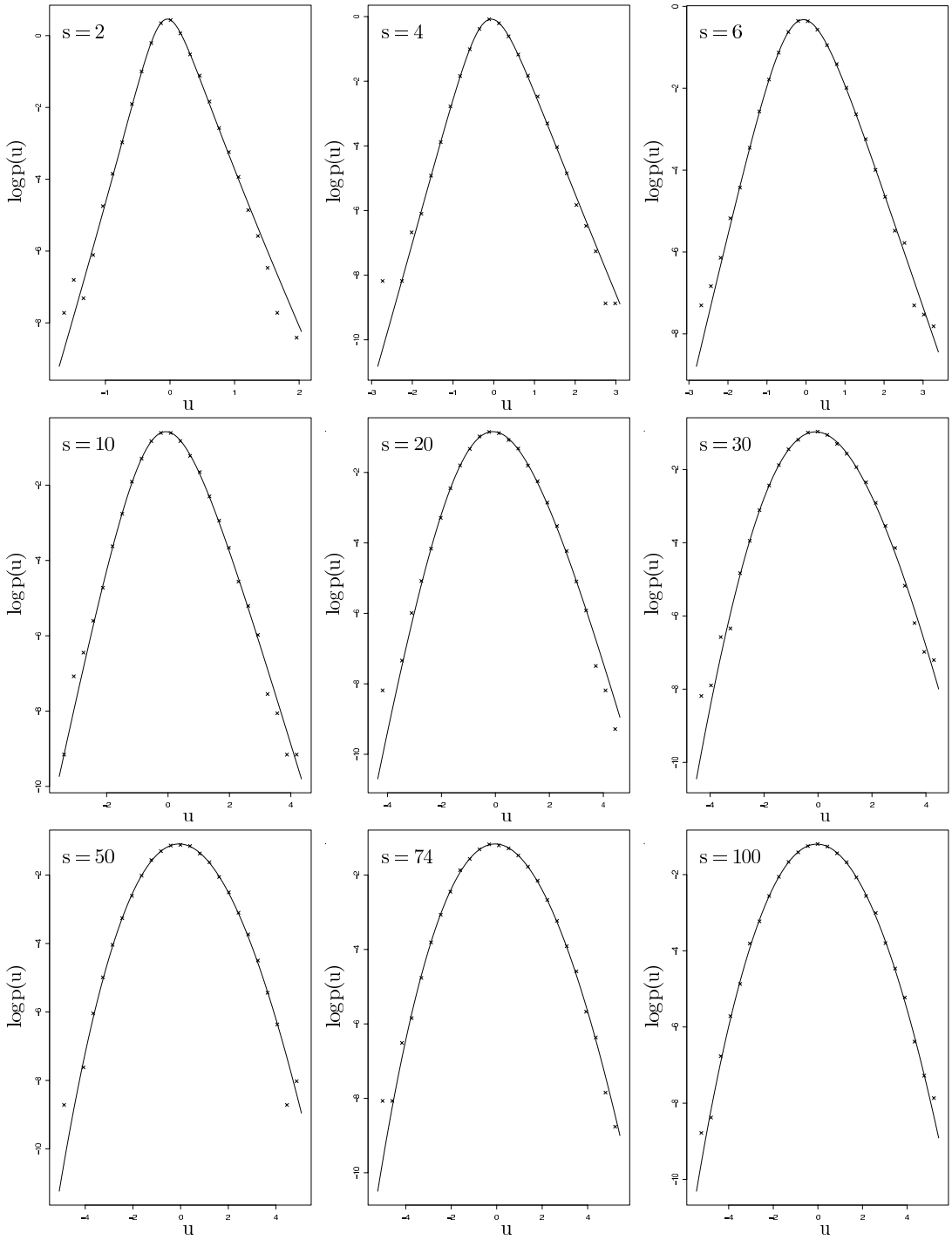

Fig. 4. Approximation of the pdf of velocity increments within the class of NIG distributions for data set III and lags $s = 2, 4, 6, 10, 20, 30, 50, 74, 100$ (in units of the finest resolution $1/f$).

as a function of the estimated scale parameter δ (Fig. 5c). We observe a striking collapse of the three sets of exponents m on one single curve. The location of each set of exponents on this common curve apparently depends on the Reynolds number and in general on the kind of large scale fluctuations. The dependence seems, however, to be weak since there is a large region where the three data sets overlap.

4 Universality and parsimony

The NIG distributions (cf. Sect. 2.1) are characterized by four parameters $\alpha(s)$, $\beta(s)$, $\delta(s)$ and $\mu(s)$ whose dependence on the lag s will be examined in the following. We mainly focus on shape triangles, introduced in Section 2.1, as a descriptive tool for the characterization of the global shape of NIG distributions, and on various combinations

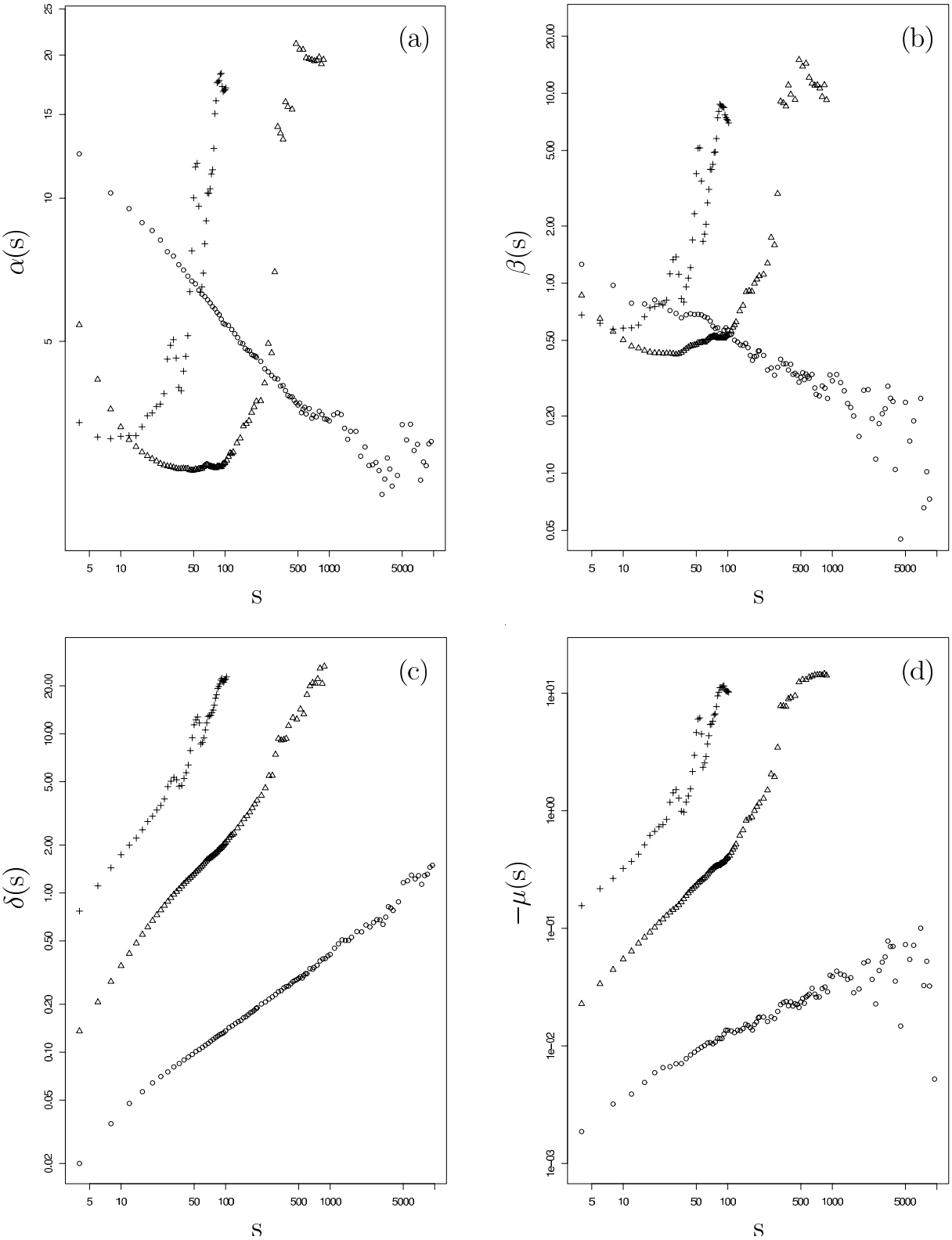

Fig. 5. Estimated parameters $\alpha(s)$, $\beta(s)$, $\delta(s)$ and $-\mu(s)$ as functions of the lag s (in units of the finest resolution $1/f$) for data set I ($\circ$), data set II ($\triangle$) and data set III ($+$) in double logarithmic representation.

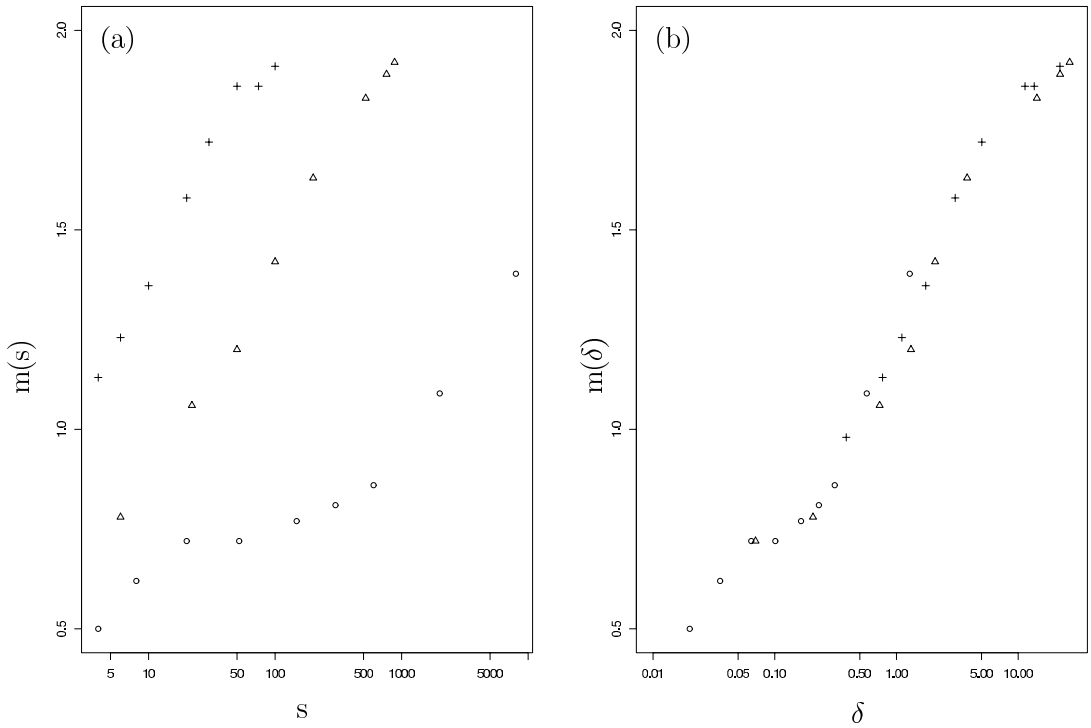

Fig. 6. Stretching exponents m as a function of the lag s (a) and as function of the scale parameter δ (b) for data set I ($\circ$), data set II ($\triangle$) and data set III ($+$). Abscissae are represented in logarithmic scales.

of the parameters that allow for a parsimonious and, to a certain extent, universal description of the fitted NIG distributions.

4.1 Shape triangles

The NIG shape triangle is a plotting device for showing the asymmetric and non-Gaussian character of a given NIG distribution. The parameters χ and ρ are associated to the degree of asymmetry of the given distribution while (χ, ξ) reflects the degree of non-Gaussianity, with the limit $(\chi, \xi) \to (0, 0)$ for a normal distribution, see Figure 1. Figures 7–9 show the shape triangles and amplifications of the relevant part of the triangles for data sets I-III. Each symbol corresponds to the maximum likelihood estimate of (ξ, χ) at one given lag s (which can be read off from Fig. 14a).

While data sets II and III clearly approach the Gaussian limit at the origin for large lags, this is not observed for data set I. The non-Gaussian behaviour for large lags for data set I already appeared in connection with the stretching exponent $m < 2$ for the tails. The difference in the large scale behaviour might be due to the fact that experiments II and III are performed under controlled and steady conditions, while experiment I involves unsteady large scale fluctuations, leading to a limit that is away from Gaussianity. However it is not clear to what extent this limit describes the dynamics of large scale fluctuations since we could not resolve all lags up to the estimated decorrelation time $T = 20000$ for data set I (Tab. 2).

Some common features are clearly visible in the shape triangles. First, we observe that the path within the shape triangle is restricted to the same region $0 \leq \chi < 0.2$, i.e. all three data sets exhibit the same kind of asymmetry, irrespective of the Reynolds number. Furthermore, we observe that the slope $1/\rho = \alpha/\beta$ (consult Eq. (10)) of all three paths across lags is roughly constant for each data set and of the same order $10-20$. Thus, the evolution of the pdf from its initial asymmetric state to its final state follows approximately a type of universal, linear behaviour. Differences show up in the initial and final states which are near the origin for data sets II and III and some other state for data set I, which is symmetric, but does not have Gaussian steepness. The initial and final state in the shape triangle clearly depend on the Reynolds number and the experimental situation. However the way these two shapes are connected across lags follows a simple, approximately linear evolution that is very similar for all three data sets.

4.2 Smooth parameters and universality

This section gives a more detailed description of the parameters of the fitted NIG distributions. The estimated values of the four parameters $\alpha(s)$, $\beta(s)$, $\mu(s)$ and $\delta(s)$ as shown in Figure 5 follow different curves for each data set. Of course, we can also choose various combinations of these parameters as our basic parameters. In the following we will focus on combinations that are smooth and have a simple, in particular monotonic dependence on the lag s. We choose the scale parameter δ, the ratio α/δ and

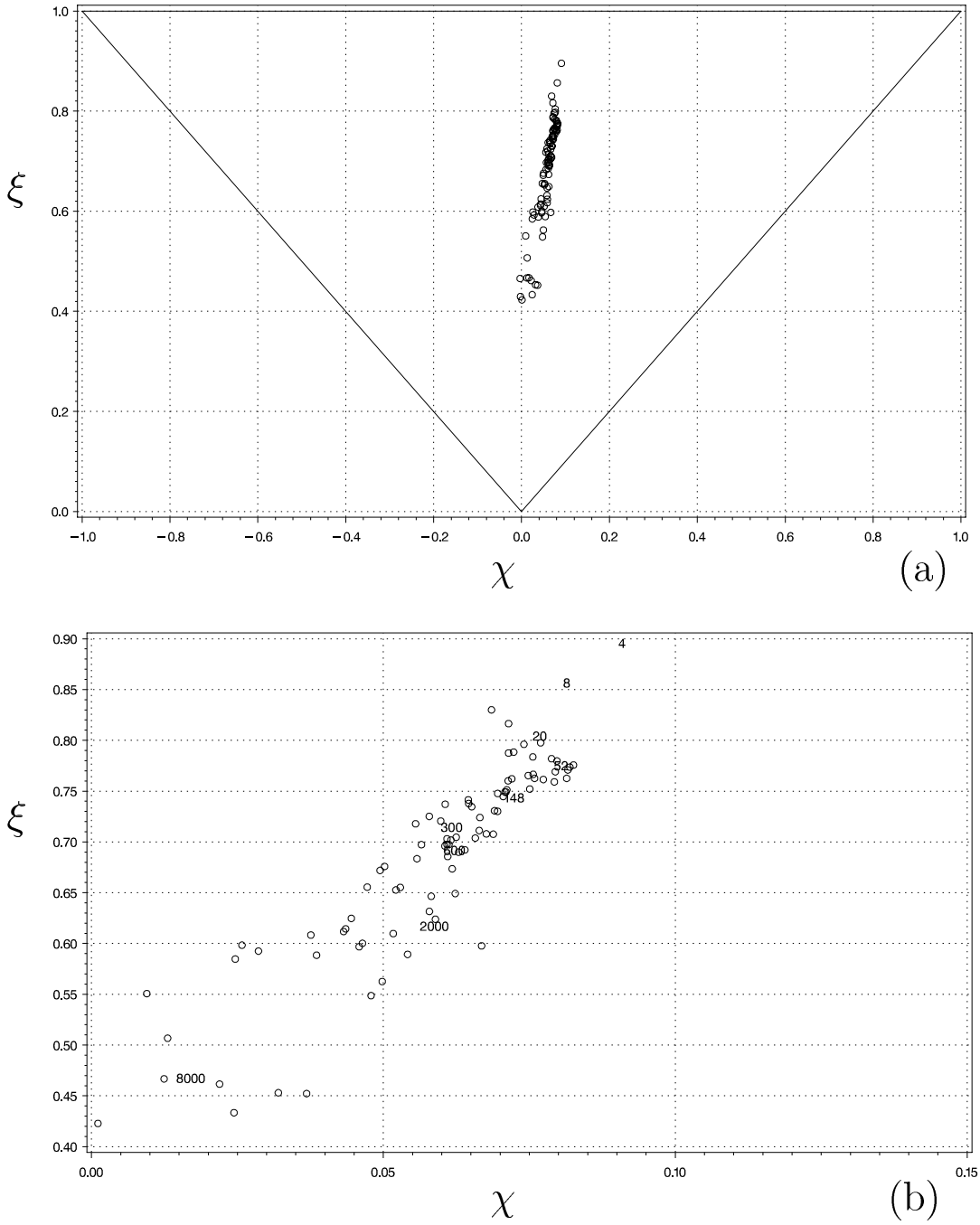

Fig. 7. (a) Shape triangle for the evolution of the pdf of velocity increments across lags for data set I. (b) Amplification of the relevant part of (a). The numbers denote the lags of several of the velocity increments, as used in Figure 1. All represented lags can be read off from Figure 14a.

the steepness ξ as the set of parameters that are convenient for our purposes. We are able to restrict to three parameters instead of four once we use the stationarity of the velocity field which implies that the cumulant of first order (5) vanishes. Thus, we expect $\mu(s)$ to be of the form

$$\mu(s) = -\frac{\delta(s)\beta(s)}{\sqrt{\alpha(s)^2 - \beta(s)^2}}. \qquad (14)$$

Figures 10–12 show $-\mu(s)$ and $\delta(s)\beta(s)/\sqrt{\alpha(s)^2 - \beta(s)^2}$ as a function of the lag s for each of our data sets. Besides some scatter for data set I, relation (14) is confirmed for all three data sets with high accuracy.

The scale parameter $\delta(s)$ as a function of the lag s is shown in Figure 5c. Leaving aside the scatter for large lags that is due to the decrease of the sample size with increasing lag, we observe a monotonically increasing function of the lag s. For intermediary lags an approximate scaling range becomes visible which increases with

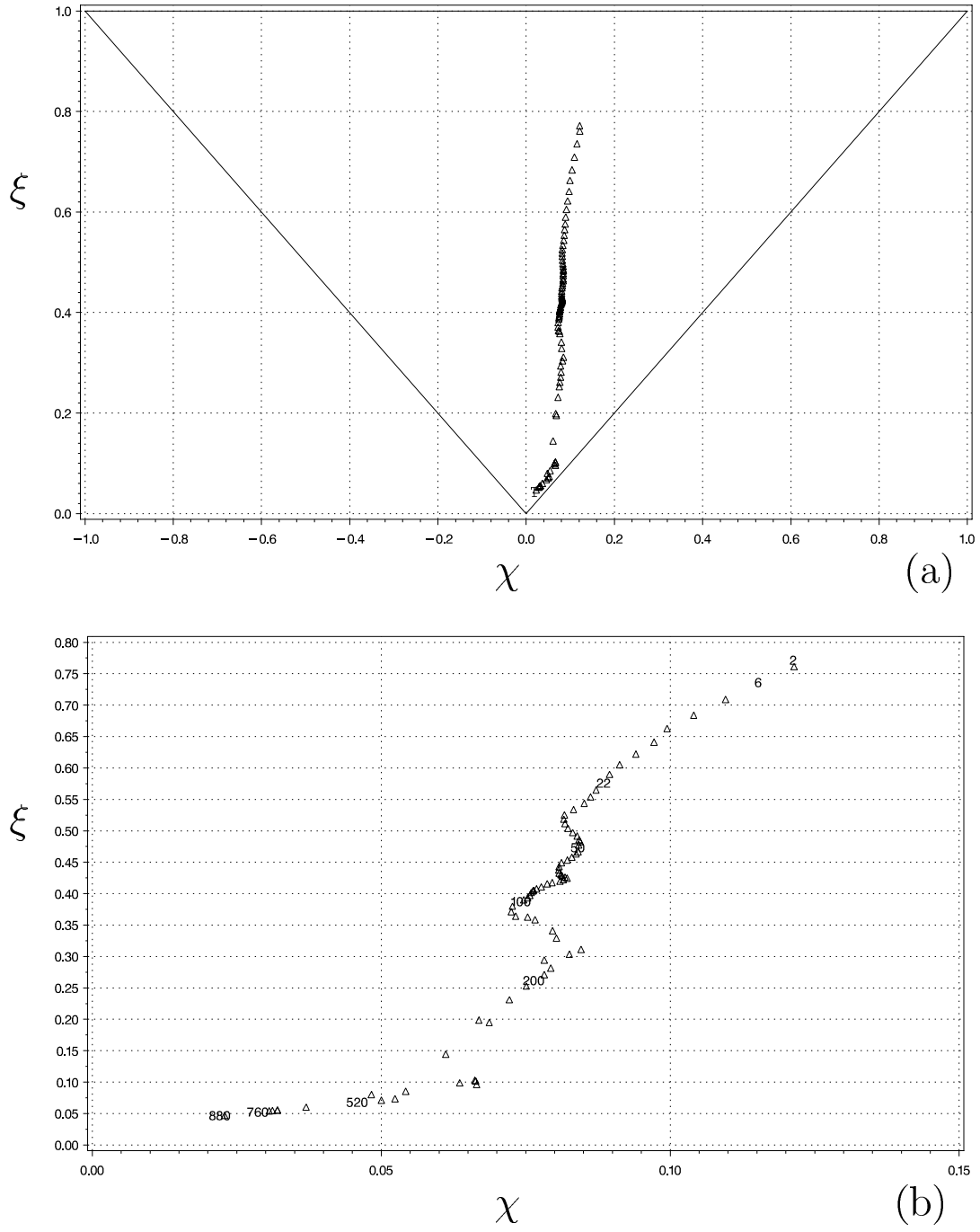

Fig. 8. (a) Shape triangle for the evolution of the pdf of velocity increments across lags for data set II. (b) Amplification of the relevant part of (a). The numbers denote the lags of several of the velocity increments, as used in Figure 1. All represented lags can be read off from Figure 14a.

increasing Reynolds number. In the following we will, in view of the monotonicity, think of $\delta(s)$ as a time change and investigate the other parameters α/δ and ξ as functions of $\delta(s)$.

The usefulness of this time change was already shown in Section 3.2 where we observed an approximate collapse of the stretching exponents $m(\delta)$ for the tails. A similar behaviour can be observed for the parameters $(\alpha/\delta)(\delta)$ and $\xi(\delta)$ in their dependence on δ. Figure 13a shows α/δ as function of the lag s and Figure 13b as a function of δ for our three data sets. For both of the two parameter sets there is a striking collapse onto one single curve. Each data set is covering a certain part of this common curve in the $(\delta, \alpha/\delta)$ space, with large overlapping regions. It is to note that the corresponding plots of α/δ as a function of the lag s (Fig. 13a) show a rather different behaviour for each data set. It is the time change with $\delta(s)$ that causes the collapse on one, apparently universal curve.

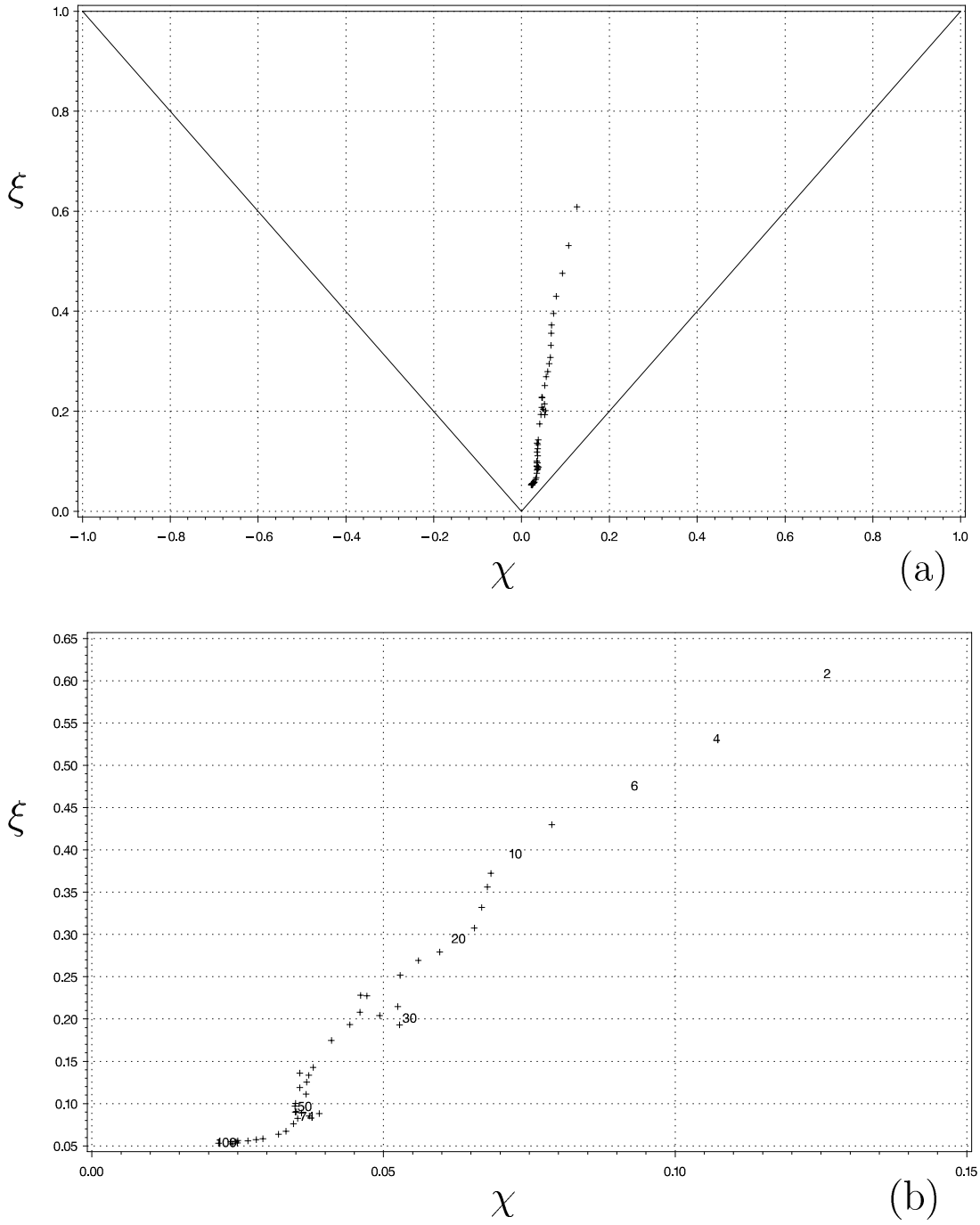

Fig. 9. (a) Shape triangle for the evolution of the pdf of velocity increments across lags for data set III. (b) Amplification of the relevant part of (a). The numbers denote the lags of several of the velocity increments, as used in Figure 1. All represented lags can be read off from Figure 14a.

A similar kind of universality can be observed for the steepness parameter ξ when plotted as a function of δ. Figure 14 shows the comparison of $\xi(s)$ as a function of the lag s and $\xi(\delta)$ as function of the scale parameter δ for all three data sets. The same striking collapse of the three parameter sets on a single, universal curve can be observed.

The collapse of the various parameter sets is not perfect, but to a first approximation it seems to hold for all lags. We come back to the accuracy of the collapse of $\xi(\delta)$ at the end of this Section. Here we state that, to a first approximation, a universal and parsimonious description of the pdf of velocity increments for all three data sets can be achieved using the three functions $\delta(s)$, $(\alpha/\delta)(\delta)$

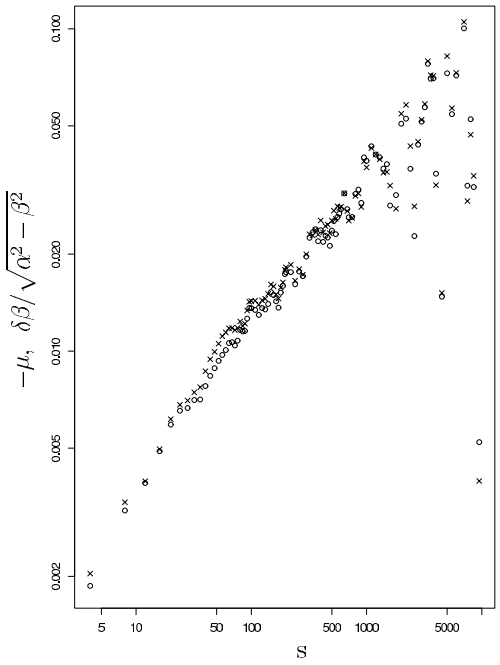

Fig. 10. Comparison of $-\mu(s)$ ($\circ$) with $\delta(s)\beta(s)/\sqrt{\alpha^2(s)-\beta^2(s)}$ ($\times$) for data set I in double logarithmic representation.

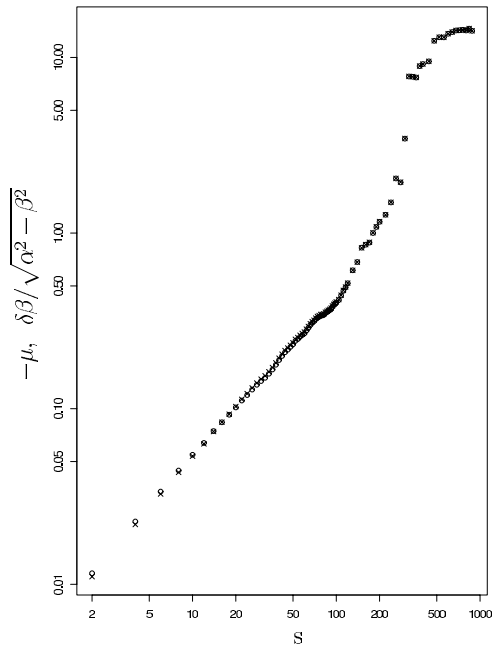

Fig. 11. Comparison of $-\mu(s)$ ($\circ$) with $\delta(s)\beta(s)/\sqrt{\alpha^2(s)-\beta^2(s)}$ ($\times$) for data set II in double logarithmic representation.

and $\xi(\delta)$ as the basic parameters to describe the evolution of the pdf across lags. The scale parameter $\delta(s)$ is the basic time change for each data set and allows for an approximately universal description of the remaining parameters. This universality is characterized by the striking fact that the parameters $(\alpha/\delta)(\delta)$ and $\xi(\delta)$ for each data set follow one universal function. It is the time change $\delta(s)$ that embodies most of the differences between the data sets.

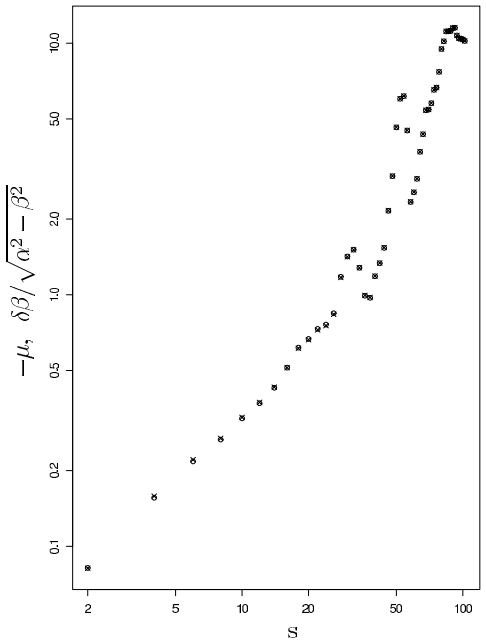

Fig. 12. Comparison of $-\mu(s)$ ($\circ$) with $\delta(s)\beta(s)/\sqrt{\alpha^2(s)-\beta^2(s)}$ ($\times$) for data set III in double logarithmic representation.

Some remarks about the interpretation of our choice of basic parameters are in order. The scale parameter $\delta(s)$ has the advantage of being monotonically increasing with the lag s and thus provides a natural time change for each data set. The parameter ξ describes the steepness of the NIG distribution and is invariant under scale-location transforms. As one of the parameters of the shape triangle it serves as a global parameter for the evolution of the shape across lags. The third parameter α/δ is closely related to the second order structure functions. In our investigation of the empirical pdf, we have $\beta \ll \alpha$ for not too large lags. Thus we approximate to first order $S_2 = \kappa_2 \approx \delta/\alpha$ (consult Eq. (5)). Universal features as shown by the collapse of α/δ are thus related to universal features of the second order structure functions. This universality even applies when there is no inertial range as for data set III. A related kind of time change that applies for inertial range statistics only, is given by the concept of Extended Self-Similarity [10]. There, some structure function of order n' serves as a time change for structure functions of higher orders $n > n'$, which leads in most cases to a more pronounced and more extended scaling behaviour of structure functions. We come back to this point in Section 5.

The universal behaviour of α/δ and ξ reveals itself as the approximate collapse of these parameters on single curves, one for α/δ and one for ξ. For α/δ we did not find a simple analytical expression for the universal shape that is visible in Figure 13b. However for the steepness ξ it is possible to detect a simple exponential behaviour

$$\xi(\delta) = \exp(-a\delta^b) \tag{15}$$

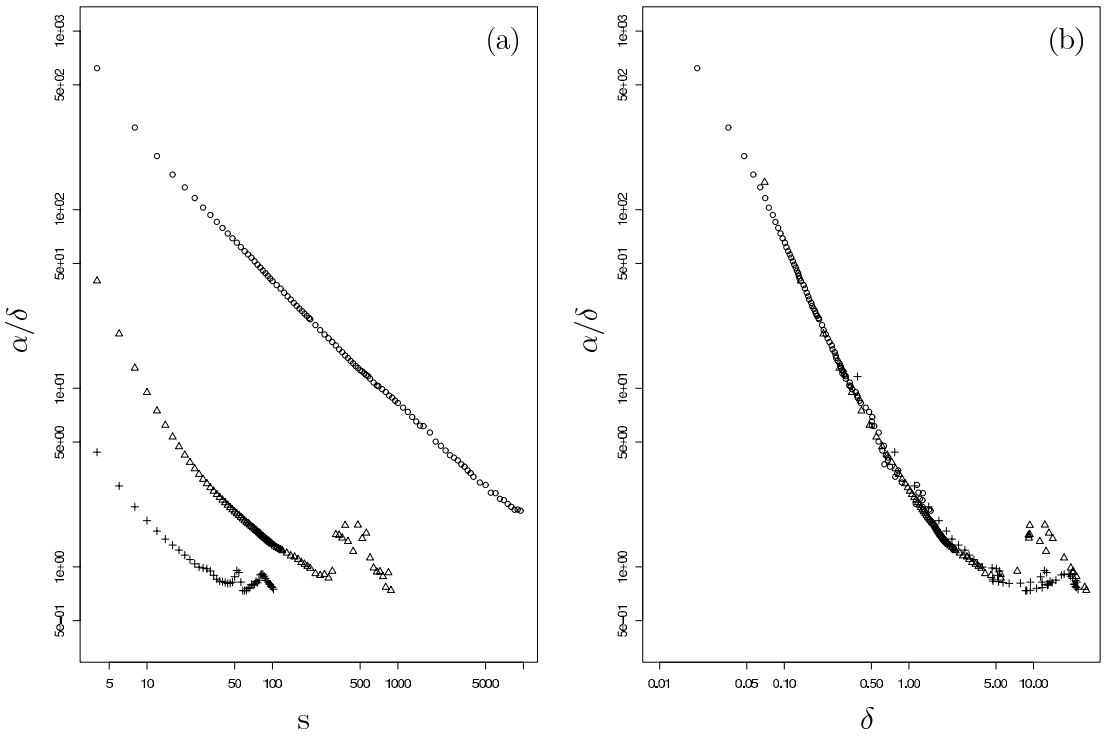

Fig. 13. (a) Comparison of $(\alpha/\delta)(s)$ as a function of the lag s with (b) $(\alpha/\delta)(\delta)$ as a function of the scale parameter δ for data set I ($\circ$), data set II ($\triangle$) and data set III ($+$) in double logarithmic representation.

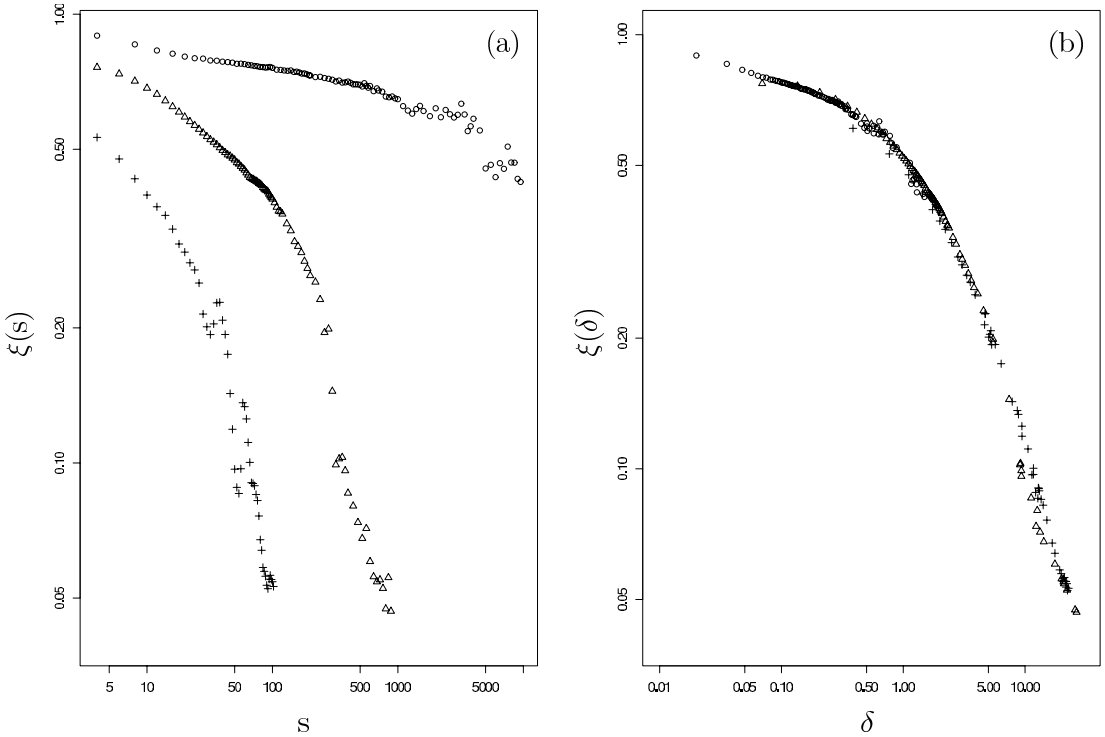

Fig. 14. (a) Comparison of $\xi(s)$ as a function of the lag s with (b) $\xi(\delta)$ as a function of the scale parameter δ for data set I ($\circ$), data set II ($\triangle$) and data set III ($+$) in double logarithmic representation.

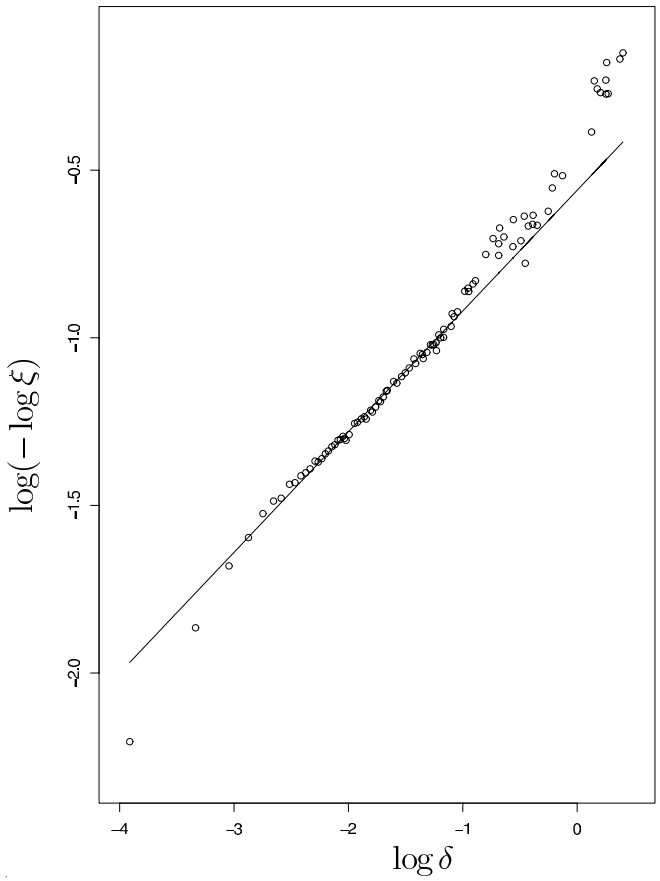

Fig. 15. Illustration of the linear dependence of $\log(-\log(\xi))$ on $\log(\delta)$ for data set I. The straight line is of the form $0.36\log(\delta) - 0.56$.

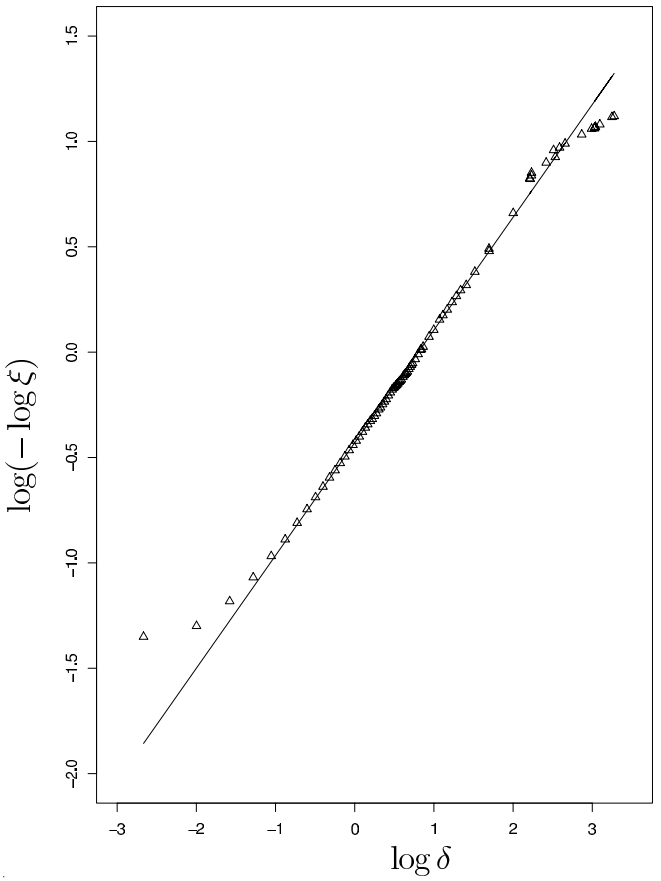

Fig. 16. Illustration of the linear dependence of $\log(-\log(\xi))$ on $\log(\delta)$ for data set II. The straight line is of the form $0.54\log(\delta) - 0.43$.

for a certain, but extended range of δ and for each individual data set. The estimated exponents b of the three data sets are different, thus indicating the limitations of the collapse of ξ on one single curve. The apparent universal shape of ξ as a function of δ is due to the fact that the curves given by the exponential laws (15), for each data set, are very close to each other with extended overlaps.

Figure 15 shows $\log(-\log(\xi))$ as a function of $\log(\delta)$ for data set I. We observe an extended range of δ-values where the exponential behaviour (15) holds to high accuracy with $a = 0.56$ and $b = 0.36$. Translating the δ coordinate back to temporal lags s (Fig. 5c), we get the range $s \in [12, 1000]$ that is over three orders of magnitude. This kind of exponential behaviour also holds for data set II and III. From Figures 16, 17, we clearly see that the exponential behaviour (15) holds for $s \in [10, 500]$ for data set II and $s \in [4, 80]$ for data set III, thus covering most of the lags we looked at in our analysis. The estimated values are $a = 0.43$, $b = 0.54$ for data set II and $a = 0.35$, $b = 0.49$ for data set III.

For the moment we do not have a theoretical explanation for this kind of exponential law. An important point in this respect is the fact that the same exponential behaviour was observed for data on wind shear consisting of changes in headwind speed experienced by aircraft during landing phase [53]. Despite the obvious fundamental difference to the kind of data we use in our analysis, there appears to be the common feature of the steepness ξ to depend exponentially on the scale parameter δ.

5 Time change and extended self-similarity

This section discusses the relation between the time change $\delta(s)$ and the concept of ESS. For convenience, subscripts i and j refer to different data sets (different experiments and/or different Reynolds numbers), superscripts $f^{(-1)}$ denote the inverse of the function f, $R(f)$ the range of f and $\stackrel{d}{=}$ denotes equality in distribution.

Due to the stationarity of the velocity field, the distribution of velocity increments $u(s)$ is completely determined by the three parameters $\delta(s)$, $(\alpha/\delta)(s)$ and $\xi(s)$. The time change $\delta(s)$ causes $(\alpha/\delta)(\delta)$ and $\xi(\delta)$ to collapse, to first order, on single, universal curves with large overlaps. Thus we propose the existence of a stochastic equivalence class

$$u_i(s_1) \stackrel{d}{=} u_j(s_2) \quad \text{if and only if} \quad F_i(s_1) = F_j(s_2), \quad (16)$$

where $F\colon\ [0,\infty) \to [0,\infty)$ is a positive real-valued function whose inverse exists. The analysis of the distribution

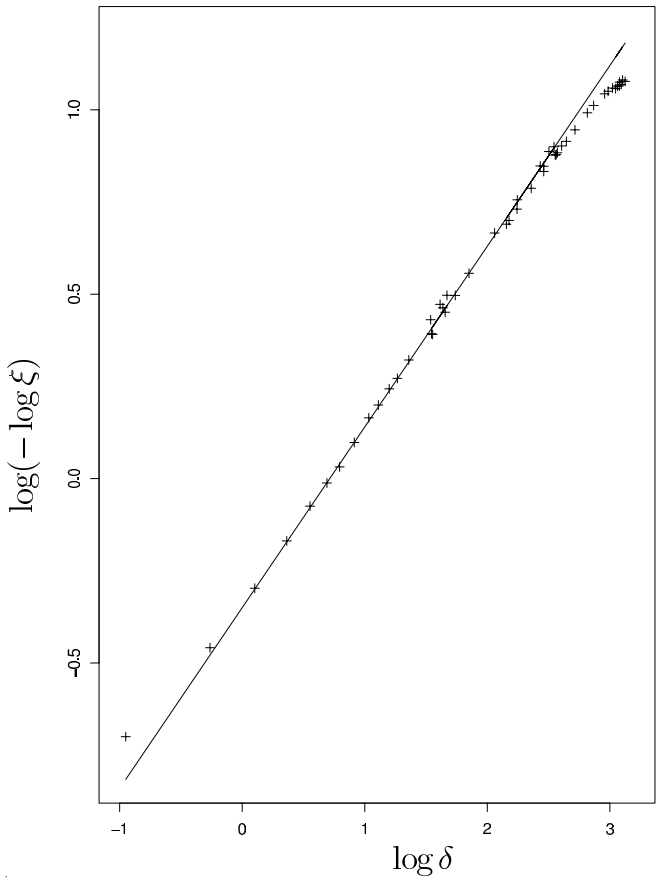

Fig. 17. Illustration of the linear dependence of $\log(-\log(\xi))$ on $\log(\delta)$ for data set III. The straight line is of the form $0.49\log(\delta) - 0.35$.

of velocity increments within the class of NIG distributions suggests

$$F_i(s) \approx \delta_i(s), \tag{17}$$

which we confirmed to a reasonable accuracy for $i \in \{\text{data set I, data set II, data set III}\}$. A closer examination of (16) and its connection to the time change $\delta(s)$ for more data sets is the subject of a forthcoming paper. For the moment we assert that our empirical findings support the existence of a stochastic equivalence relation (16).

We may rewrite (16) for $s \in R(F_i) \cap R(F_j)$ as

$$u_i(s) \stackrel{d}{=} u_j(F_j^{(-1)}(F_i(s))) = u_j(F_{i,j}(s)) \tag{18}$$

where

$$F_{i,j}(s) = F_j^{(-1)}(F_i(s)). \tag{19}$$

In particular, if j refers to a fully developed turbulent velocity field, (18) directly compares the dynamics of the fully developed state with that of any finite Reynolds number if the Functions $F_i(s)$ and $F_j(s)$ are known.

In the following we discuss the equivalence relation (16) with respect to ESS. ESS states that for structure functions $\mathrm{S}_{i,n}(s) = \mathrm{E}\{u_i(s)^n\}$ of order n, $n \in \mathbb{N}$, we have

$$\mathrm{S}_{i,n}(s) = c_i(n)(f_i(s))^{\tau(n)} \tag{20}$$

for a certain range of scales that extends the inertial range. The important point here is that the real-valued functions $f_i\colon\ [0,\infty) \to [0,\infty)$ do not depend on n. $c_i(n)$ denotes a constant that depends on i and n. Note that with our definition of velocity increments (12) we may assume $c_i(n) \geq 0$.

Under mild assumptions it is possible to show the equivalence of the ESS relation (20) and the existence of an equivalence class (18). The proof of (18)⇒(20) only requires the existence of a fully developed turbulent state where the scaling relation (1) holds. The proof of (20)⇒(18) additionally needs the assumption of finite structure functions $\mathrm{S}_n(s) < \infty$ for all $n \in \mathbb{N}$.

Starting from (18), it follows immediately that

$$\mathrm{S}_{i,n} = S_{j,n}(F_j^{(-1)}(F_i(s))). \tag{21}$$

For j referring to a fully developed turbulent velocity field where (1) is assumed to hold, we get

$$\mathrm{S}_{i,n} = (F_j^{(-1)}(F_i(s)))^{\tau(n)}. \tag{22}$$

Comparing (22) with (20), we conclude

$$f_i(s) \propto F_j^{(-1)}(F_i(s)). \tag{23}$$

Thus ESS follows straightforward from (18).

In the next step, we show that ESS implies the equivalence relation (18) under the assumption that all structure functions $\mathrm{S}_n(s)$, $n \in \mathbb{N}$ are finite. This assumption means (in essence) that the distribution of velocity increments is determined by all its finite moments.

Again, choosing for j a fully developed turbulent state where (1) holds, we rewrite the ESS relation (20) as

$$\mathrm{S}_{i,n}(s) \propto \mathrm{S}_{j,n}(f_i(s)). \tag{24}$$

Since the structure functions of arbitrary integer order are assumed to be finite, we get from (24) (ignoring the constant of proportionality in (24))

$$u_i(s) \stackrel{d}{=} u_j(f_i(s)). \tag{25}$$

Note that in (25) (as well as in (23)) j refers to a fully developed turbulent state. For an arbitrary state j, (25) translates to

$$u_i(s) \stackrel{d}{=} u_j(f_j^{(-1)}(f_i(s))) \tag{26}$$

and comparing (18) with (26) we obtain

$$F_{i,j}(s) = f_j^{(-1)}(f_i(s)). \tag{27}$$

Thus, ESS implies the existence of an equivalence relation (18) and the proof of the equivalence of (20) and (18) is completed.

To our knowledge, the reformulation of ESS in terms of an equivalence relation of the form (18) has not been reported in the literature so far. Although it is straightforward to reach (18) starting from (20), the character

of (18) is completely different. While (20) relates structure functions within the same experiment, (18) relates the statistics of different experiments.

It is to note that we were able to deduce the functions $F_{i,j}$ starting from (20), but this does not determine the functions F_i. Our empirical analysis suggests the scale parameter δ_i as an approximation for F_i, which is not implied by ESS.

6 Conclusions

We performed a statistical analysis of the pdf of turbulent velocity increments for three rather different data set, different in experimental conditions and in Reynolds number. We found that the pdf of velocity increments can be well fitted within the class of NIG$(\alpha, \beta, \mu, \delta)$ distributions for all lags, from the finest resolution up to the largest lags that allow for a proper statistical estimation of the parameters α, β, μ and δ. The resolution of the tails was shown to be in conformity with classical findings, that is an evolution of the tails from stretched exponentials to Gaussian-like shapes. The illustrative representation of the evolution of the shape of the pdf across lags with the help of shape triangles revealed a simple, linear and universal behaviour for all three data sets.

The analysis within the class of NIG distributions comes with four parameters α, β, μ and δ, where one, chosen to be μ, depends on the other three parameters α, β and δ in a precise way due to the stationarity of the velocity data. The remaining three parameters $\alpha(s)$, $\beta(s)$ and $\delta(s)$ as functions of the lag s depend on s in a non-universal way. However, once we introduce a time change, from s to $\delta(s)$, striking universal features can be detected.

It turns out that maximum likelihood estimates of the parameter combinations α/δ and ξ, when plotted as functions of the scale parameter δ, collapse (to first order) on single, apparently universal curves, one for α/δ and one for ξ, with large overlapping regions. The individual characteristics of each data set are thus largely captured by the scale parameter $\delta(s)$. In addition, we find that the stretching exponents m describing the tails of the pdf also collapse on one single curve when plotted as a function of the scale parameter δ. Note that we normalised each data set by its standard deviation. However, it does not change the form of the functional dependence of α/δ, ξ and m on the scale parameter δ.

In summary we are able to parsimoniously describe all three data sets by two universal curves and one individual time change $\delta(s)$ for each data set.

We were able to show the existence of a simple exponential behaviour for $\xi(\delta)$ for a wide range of δ values. This exponential law seems to have far-reaching applicability since it is also reported for a rather different kind of turbulent data set.

The universal features we were able to show for turbulent velocity increments goes far beyond the usual multifractal description which in general is appropriate only for a restricted range of lags (a fraction of the inertial range) and very high Reynolds numbers, where universal scaling exponents $\tau(n)$ for structure functions (1) are expected. Our three data sets covered a range of Reynolds numbers where, on the one hand, an inertial range was clearly visible (data sets I and II), while on the other hand, no inertial range could be detected (data set III). Thus, our findings concerning universal features of the distributional properties of velocity increments apply without reference to inertial range dynamics.

For the moment, our analysis has to be understood as a purely empirical study. We have no clear physical interpretation of why the time change $\delta(s)$ works so surprisingly well in detecting universal features for the pdf of turbulent velocity increments. There is a whole range of challenging problems that immediately come to mind.

We demonstrated the relation of the time change $\delta(s)$ to the concept of Extended Self-Similarity. Our empirical findings suggest, in accordance with ESS, the existence of a fundamental equivalence class that relates the statistics of velocity increments of different Reynolds numbers and different experiments. In this respect, the closer examination of the function F is of particular importance.

The analysis of more data sets is needed to shed light on the dependence of the time change $\delta(s)$ on the Reynolds number and on the kind of experiment that is performed. Another important point concerns the similarities between our data sets and the one that is described in [53]. Both sets of data show the same exponential law (15).

A third issue concerns the implications of our results for the understanding of the dependence structure of the velocity field. We intend to study the dependence structure in subsequent work.

We are much indebted to K.R. Sreenivasan, J. Peinke and B.R. Pearson for allowing us to use the data sets I, II and III, respectively. We are also grateful to the two referees of this paper for helpful comments. Part of this work was supported by MaPhySto – A Network in Mathematical Physics and Stochastics, funded by the Danish National Research Foundation. J.S. acknowledges support from the Alexander von Humboldt Foundation with a Feodor-Lynen-Fellowship.

References

1. A.N. Kolmogorov, Dokl. Akad. Nauk. SSSR **30**, 9 (1941)
2. A.N. Kolmogorov, Dokl. Akad. Nauk. SSSR **32**, 16 (1941)
3. A.N. Kolmogorov, J. Fluid Mech. **13**, 82 (1962)
4. A.M. Obukhov, Dokl. Akad. Nauk SSSR **32**, 22 (1941)
5. A.M. Obukhov, Izv. Akad. Nauk SSSR Ser. Geogr. Geofiz **5**, 453 (1941)
6. A.M. Obukhov, J. Fluid Mech. **13**, 77 (1962)
7. U. Frisch, *Turbulence. The legacy of A.N. Kolmogorov* (Cambridge University Press, 1995)
8. K.R. Sreenivasan, R.A. Antonia, Ann. Rev. Fluid Mech. **29**, 435 (1997)
9. A. Arneodo et al., Europhys. Lett. **34**, 411 (1996)
10. R. Benzi et al., Phys. Rev. E **48**, 29 (1993)
11. V.R. Kuznetsov, V.A. Sabelnikov, *Turbulence and Combustion* (Hemisphere Publishing Corporation, New York, 1990)

12. B. Castaing, Y. Gagne, E.J. Hopfinger, Physica D **46**, 177 (1990)
13. Y. Gagne, M. Marchand, B. Castaing, J. Phys. II France **4**, 1 (1994)
14. B. Chabaud et al., Phys. Rev. Lett. **73**, 3227 (1994)
15. A. Praskovsky, S. Oncley, Phys. Rev. Lett. **73**, 3399 (1994)
16. A. Vincent, M. Meneguzzi, J. Fluid Mech. **225**, 1 (1991)
17. P. Kailasnath, K.R. Sreenivasan, G. Stolovitzky, Phys. Rev. Lett. **68**, 2766 (1992)
18. G. Stolovitzky, K.R. Sreenivasan, A. Juneja, Phys. Rev. E **48**, R3217 (1993)
19. P. Tabeling et al., Phys. Rev. E **53**, 1613 (1996)
20. G.S. Lewis, H.L. Swinney, Phys. Rev. E **59**, 5457 (1999)
21. A. Noullez et al., J. Fluid Mech. **339**, 287 (1997)
22. W. van de Water, J. Herweijer, J. Fluid Mech. **387**, 3 (1999)
23. R. Benzi et al., Phys. Rev. Lett. **67**, 2299 (1991)
24. J.M. Tchéou et al., Physica D **129**, 93 (1999)
25. T. Arimitsu, N. Arimitsu, preprint: `cond-mat/0110349` (2001)
26. T. Arimitsu, N. Arimitsu, preprint: `cond-mat/0109007` (2001)
27. T. Arimitsu, N. Arimitsu, preprint: `cond-mat/0109132` (2001)
28. T. Arimitsu, N. Arimitsu, Physica A **259**, 177 (2001)
29. C. Beck, Physica A **277**, 115 (2000)
30. C. Beck, G.S. Lewis, H.L. Swinney, Phys. Rev. E **63**, 035303 (2001)
31. C. Renner, J. Peinke, R. Friedrich, J. Fluid Mech. **433**, 383 (2001)
32. O.E. Barndorff-Nielsen, Research Report **300**, Dept. Theor. Statistics, Aarhus University (1995)
33. O.E. Barndorff-Nielsen, Scand. J. Stat. **24**, 1 (1997)
34. O.E. Barndorff-Nielsen, in *Probability Towards 2000. Proceedings of a Symposium held 2-5 October 1995 at Columbia University*, edited by L. Acccardi, C.C. Heyde (Springer, New York, 1998), p. 47
35. O.E. Barndorff-Nielsen, Finance and Stochastics **2**, 41 (1998)
36. O.E. Barndorff-Nielsen, Theory Prob. Its Appl. **45**, 175 (1998)
37. T.H. Rydberg, Comm. Stat.: Stochastic Models **13**, 887 (1997)
38. T.H. Rydberg, Math. Finance **9**, 183 (1999)
39. K. Prause, Dissertation, Albert-Ludwigs-Universität, Freiburg i. Br. 1999
40. E. Eberlein, in *Lévy Processes – Theory and Applications*, edited by O.E. Barndorff-Nielsen, T. Mikosch, S. Resnick (Birkhäuser, Boston, 2000), p. 319
41. S. Raible, Dissertation, Albert-Ludwigs-Universität, Freiburg i. Br. 2000
42. O.E. Barndorff-Nielsen, N. Shephard, J. R. Stat. Soc. B **63**, 167 (2001)
43. O.E. Barndorff-Nielsen, N. Shephard, in *Lévy Processes – Theory and Applications*, edited by O.E. Barndorff-Nielsen, T. Mikosch, S. Resnick (Birkhäuser, Boston, 2001), p. 283
44. O.E. Barndorff-Nielsen, N. Shephard, Scand. J. Stat. **30**, 277 (2002)
45. O.E. Barndorff-Nielsen, K. Prause, Finance and Stochastics **5**, 103 (2001)
46. O.E. Barndorff-Nielsen, S.Z. Levendorskiĭ, Quantitative Finance **1**, 318 (2001)
47. S. Asmussen, J. Rosinski, J. Appl. Probab. **38**, 482 (2001)
48. R. Cont, P. Tankov, *Financial Modelling With Jump Processes* (Chapman & Hall/CRC, London, 2004)
49. O.E. Barndorff-Nielsen, Proc. R. Soc. London A **353**, 401 (1977)
50. B. Dhruva, Ph.D. Thesis, Yale University, 2000
51. K.R. Sreenivasan, B. Dhruva, Prog. Theor. Phys. Suppl. **130**, 103 (1998)
52. R.A. Antonia, B.R. Pearson, Phys. Rev. E **62**, 8086 (2000)
53. O.E. Barndorff-Nielsen, J.L. Jensen, M. Sørensen, Boundary-Layer Meteorology **49**, 417 (1989)